ANALYSIS OF TRANSIENT RADIATIVE HEAT TRANSFER USING HIGH BOUNDED SCHEME OF THE FT*n* FINITE VOLUME METHOD

Kamel Guedri *, Hamza Ahmed Ghulman, and Abdulmajeed Saeed Al-Ghamdi
*Author for correspondence
Mechanical Engineering Department,
Faculty of Engineering and Islamic Architecture,
Umm Al-Qura University, B. Po. 5555,
Makkah, 21955, Kingdom of Saudi Arabia,
E-mails: kmguedri@uqu.edu.sa, kamel.guedri@enim.rnu.tn

ABSTRACT

In this work, the transient behavior of the absorbing, emitting, and isotropically scattering medium in radiative equilibrium is examined, using the FT*n* Finite Volume Method (FT*n*FVM), in terms of temporal and spatial evolutions of the incident radiation, radiative heat flux, and temperature of the medium. Commonly used convection schemes in computational fluid dynamics (CFD) such as STEP and CLAM are introduced for spatial discetization of the transient radiative transfer equation (TRTE). Also a non-uniform (FT*n*) angular scheme is used to capture the physics of the radiative wave propagation. The present approach is then validated by comparing with published data and applied to problems of three-dimensional isotropically participating media. It is shown that the FT*n* FVM reduces largely the ray effects. Also, the false scattering is largely remedied using the CLAM scheme is applied for the angular discretization. In all computations, the CLAM scheme produces more accurate results (with coarse grid) than the step scheme. Using the same (relatively coarse) spatial grid, the CLAM scheme captures the steep gradients and penetration depths more accurately than the step scheme. Then, effects of the scattering albedo and the optical thickness on the incident radiation distributions are presented and discussed.

.

INTRODUCTION

In traditional engineering studies, such as in the thermal analysis of furnaces, boilers, internal combustion engines, etc., the temporal variations in thermal quantities of interest are much slower than the time scale associated with the propagation of radiation. Thus, the transient term of the radiative transfer equation (RTE) can be neglected [1]. Using this assumption does not lead to important errors since the temporal variations of the observables quantities are slow as compared to the speed of light. However in many new applications [2-4], such as micro/nano-scale systems, short-pulsed laser in materials, and optical imaging in biomedicine, the transient effect must be considered in the RTE. Thus, the time derivative of the radiative intensity in the transient radiative transfer equation (TRTE) has become increasingly important and can no longer be neglected since its order of magnitude becomes comparable to that of the other terms. A detailed review on the transient radiative heat transfer can be found in Kumar and Mitra [5].

In steady radiative transfer for simple and complex configurations, the FTn FVM was tested and formulated, using the bounded high-resolution CLAM schema, by Guedri and co-authors [6,7]. They demonstrate that the FT*n* FVM has more uniform distribution of the discretized control angles then the standard FVM and it satisfies the zero and the first moment as well as the half range flux condition. Nevertheless, to our knowledge these high-order schemes have not been formulated, tested and applied for transient radiative heat transfer. Thus, an important concern of this paper is the originality of our three-dimensional formulation of this problem. This formulation is based on the FT*n* finite volume method (FT*n* FVM) and the bounded high-resolution CLAM schema. The time-dependent FT*n*-FVM is formulated, tested and applied for transient radiative transfer in absorbing, scattering and emitting three-dimensional (3D) rectangular medium. The FT*n* FVM with CLAM spatial schema is adopted in most calculations. Both the temporal and spatial evolutions of radiative heat flux and incident radiation are computed. The unsteady state solutions are validated against the data available in the literature. Also, comparisons against STEP and standard FVM results are presented and discussed. Then, the effects of scattering albedo and optical thickness on the incident radiation distributions are studied.

NOMENCLATURE

a	[-]	coefficient of the discretized equations
b	[-]	source term of the discretized equations
c	[m/s]	speed of light
G	[W/m^2]	incident radiation
I	[W/m^{2}sr]	radiant intensity

I_b	[W/sr]	black body radiant intensity
L	[-]	total number of discrete solid angles
N	[-]	dimensionless quantity
N	[-]	dimensionless quantity defined in Eq. (4)
N_θ	[-]	number of angular discretization in the polar angle
Ne	[-]	number of angular discretization in the azimuthal angle
$\boldsymbol{n}$	[-]	unit vector normal to the control volume surface
q	[W/m²]	radiative heat flux
t	[s]	Time
T	[K]	Temperature
x, y, z	[m]	Cartesian coordinates
Greek symbols		
β	[m-¹]	extinction coefficient
ΔA	[m²]	area of a control volume face
Δv	[m³]	control volume
$\Delta \Omega$	[sr]	control solid angle
Δt_c	[-]	dimensionless characteristic time step
ε	[-]	Emissivity
κ	[-]	absorption coefficient
τ	[-]	optical thickness
ω	[-]	Scattering albedo

MATHEMATICAL FORMULATION

The energy balance for the radiation energy traveling in the direction of $\boldsymbol{\Omega}$ at location s (figure 1), under assumption of gray and isotropically medium, can be written as [2-4]

$$\frac{1}{c}\frac{\partial I^l}{\partial t} + \frac{\partial I^l}{\partial s} = \kappa I_b - \kappa I^l - \sigma_s I^l + \frac{\sigma_s}{4\pi}\int_{4\pi} I^{l'} d\Omega^{l'} \quad (1)$$

Eq. (1) is the transient radiative transfer equation (TRTE) for gray medium, which is often rewritten in terms of nondimensional optical thickness

$$\tau = \int_0^s (k + \sigma_s)ds = \int_0^s \beta ds \qquad (2)$$

where $\beta = \kappa + \sigma_s$ is the extinction coefficient of the medium, leading to

$$\frac{1}{\beta \cdot c}\frac{\partial I^l}{\partial t} + \frac{\partial I^l}{\partial \tau} = -I^l + (1-\omega)I_b + \frac{\omega}{4\pi}\int_{4\pi} I^{l'} d\Omega^{l'} \quad (3)$$

NUMERICAL FORMULATION

In the finite volume method, the choice of the distribution of the directions is free; consequently it is possible to model without large difficulty the problems in which the medium receives an external radiation. The problems "ray effect" and "false scattering " encountered with the SN method also are met with the finite volume method. The FTn finite volume method (FTn FVM), proposed by Kim and Huh [8], is a new angular discretization scheme of the finite volume method. In this new angular discretization, the total number of the control angles is therefore given as $n(n + 2)$ where the polar angle is divided

uniformly into even number, n, while the azimuthal angle is uniformly divided into the numbers of the sequence of 4, 8, 12, ..., 2n, 2n, ..., 12, 8, 4 in each level of the polar angle as shown in figure 1. Kim and Hush [8] and Guedri et al. [6,7] demonstrate that the FTn FVM has more uniform distribution of the discretized control angles than the standard FVM and it satisfies the zero and the first moment as well as the half range flux condition. They showed, also, that the FTn FVM model produces more accurate results with coarse total number of the control angles. The difference between the results of the FTn FVM and the standard FVM is attenuated as the optically thick diffusion limit.
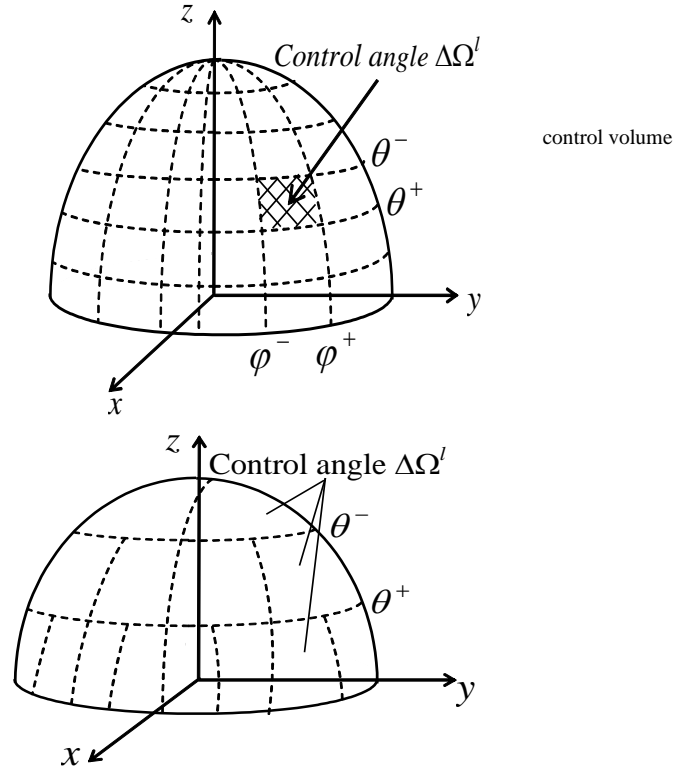

Figure 1 A typical control angle: (*a*) for standard FVM; (*b*) for the FTn FVM control angle

The linearised TRTE can be written as [4],

$$\frac{1}{\beta \cdot c}\frac{\partial I^l}{\partial t} + \frac{1}{\beta}\frac{\partial I^l}{\partial s} = -\beta_m^l I^l + S_m^l \qquad (4)$$

where the modified extinction coefficient is

$$\beta_m^l = \left(1 - \frac{\omega}{4\pi}\Delta\Omega^l\right) \qquad (5)$$

and the modified source term is

$$S_m^l = (1-\omega)I_b + \frac{\omega}{4\pi}\sum_{\substack{l'=1 \\ l'\neq l}}^M I^{l'}\Delta\Omega^{l'} \qquad (6)$$

The integration of Eq. (4), over a typical control volume, V_P, and a control angle, $\Delta\Omega^l$, within a specified time step, t, can be written as follows

$$\int\limits_{\Delta\Omega^l}\int\limits_{V_P}\int\limits_{\Delta t^*}\frac{\partial I^l}{\partial t^*}\,dt^*\,dV\,d\Omega$$

$$+\frac{1}{\beta}\int\limits_{\Delta\Omega^l}\int\limits_{V_P}\int\limits_{\Delta t^*}\frac{\partial I^l}{\partial s}\,dt^*\,dV\,d\Omega \qquad (7)$$

$$=\int\limits_{\Delta\Omega^l}\int\limits_{V_P}\int\limits_{\Delta t^*}\left(\beta_m^l I^l + S_m^l\right)dt^*\,dV\,d\Omega$$

where the dimensionless time $t^* = \beta \times c \times t$ and the dimensionless time step $\Delta t^* = \beta \times c \times \Delta t$.

The FTn Finite Volume Method (FTn FVM) is applied to discretized equation (7) where the magnitude of intensity is assumed to be constant over the control volume and a control angle. Using the fully implicit scheme, Eq. (7) can be written

$$\left(I_P^l - I_P^{l0}\right)V_P\Delta\Omega^l + \frac{1}{\beta}\sum_{i=1}^{6}I_i^l A_i \Delta t^* \int\limits_{\Delta\Omega^l}(\hat{s}\cdot\hat{n})\,d\Omega^l$$

$$= \left(-\beta_m^l I_P^l + S_m^l\right)V_P\Delta\Omega^l\Delta t^* \qquad (8)$$

where I_P^{l0} and I_P^l are the nodal intensities at the previous and at the new time step, respectively.

Eq. (8) can be rewritten as follows

$$\frac{\left(I_P^l - I_P^{l0}\right)V_P\Delta\Omega^l}{\Delta t^*} + \frac{1}{\beta}\begin{pmatrix} I_w^l A_w N_w^l + I_e^l A_e N_e^l + \\ I_s^l A_s N_s^l + I_n^l \Delta A_n N_n^l + \\ I_b^l A_b N_b^l + I_t^l A_t N_t^l \end{pmatrix}$$

$$= \left(-\beta_m^l I_P^l + S_m^l\right)V_P\Delta\Omega^l \qquad (9)$$

where

$$N_i^l = \frac{1}{\Delta\Omega^l}\int\limits_{\hat{s}^l}\hat{s}\cdot\hat{n}\,d\Omega \quad \text{for } i = w, e, s, n, b \text{ and } t \qquad (10)$$

In these equations, I_w^l, I_s^l and I_b^l are the radiation intensities on the upstream interfaces in the direction, $\hat{s}^l$. I_e^l, I_n^l and I_t^l are those on the downstream interfaces in this same direction. The subscripts, w, e, s, n, b, and t, denote west, east, south, north, bottom and top surfaces of the control volume, V_P, respectively. M and A_i represents the total number of discrete solid angles and the area of the control-volume face I, respectively.

The interface intensity at a control volume face can be assigned using an interpolation or extrapolation involving the nodal intensity at one or more of the neighbor grid points of the corresponding interface. The CLAM scheme is an abbreviation of the Curved-Line Advection Method developed for fluid flow problems [6,7,10-12]. To reduce the false scattering, the CLAM scheme is applied to radiative heat

transfer problems by Chai et al. [9,10], Coelho et al. [11,12], Guedri et al. [6] and Borjini et al. [7]. Using the CLAM scheme, the interpolation involves three nodes stencil: two upstream nodes and one downstream node (Figure 2). For the CLAM scheme, the normalized interpolation adopted is defined by [6,7,9-12]:

$$\begin{cases} \tilde{I}_w = \tilde{I}_W(2 - \tilde{I}_W) & \text{for } 0 < \tilde{I}_W < 1 \\ \tilde{I}_w = \tilde{I}_W & \text{for the rest} \end{cases} \qquad (11)$$
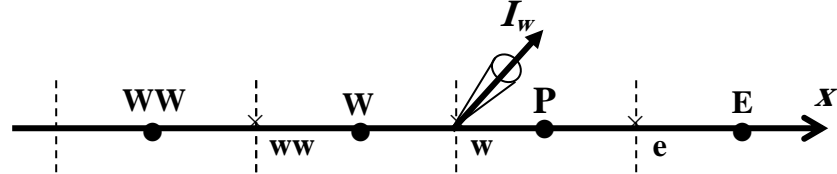
Figure 2 Upstream and downstream nodes of W control volume for x-direction.

The coefficients for other interfaces e, s, n, b and t and for other directions can be obtained without any new concepts. After assembling radiation intensities at all interfaces in the equation (9), the final discretization equation can be expressed as

$$a_P^l I_P^l = a_W^l I_W^l + a_E^l I_E^l + a_S^l I_S^l + a_N^l I_N^l + a_B^l I_B^l + a_T^l I_T^l + b_P^l$$

where

$$a_I^l = A_i \left\| -N_i^l, 0 \right\| \qquad i = w, e, s, n, b \text{ and } t$$

$$a_P^l = A_i \sum_i^{nb}\left\| N_i^l, 0 \right\| + \beta\,V_P + \frac{\Delta\Omega^l V_P}{\Delta t^*} + S_{C,\text{CLAM}}; \qquad nb$$

= all neighbors

$$b_P^l = \beta R_P^l\,V_P + \frac{\Delta\Omega^l V_P}{\Delta t^*}I_P^{l0} + S_{P,\text{CLAM}} \qquad (12)$$

In these equations, a and b are the coefficients of the discretized equation. It is noted that the symbol $\|a, b\|$ return the maximum value from a and b. The source terms due to the CLAM scheme are given as [6,7].

The STEP scheme is obtained by setting the source terms, due to the CLAM scheme, equal to zero: $S_{C,CLAM} = 0$ and $S_{P,CLAM} = 0$. For both STEP and CLAM schemes, the discretized boundary condition for a diffusely emitting and reflecting wall can be denoted by

$$I_w^l = \varepsilon_w I_b + \frac{1-\varepsilon_w}{\pi}\int\limits_{\Omega'\cdot\mathbf{n_w}<0}I_w^{l}\left|N_w^l\right|\Delta\Omega^{l'} \qquad (14)$$

In all computations, the iterative solution is terminated when the following convergence is attained

$$\left\|I_P^n - I_P^{n-1}\right|/I_P\right\| \le 10^{-5} \qquad (15)$$

where n is the number of iteration.

RESULTS AND DISCUSSION

The test case deals with a three-dimensional cubic enclosure of a non-emitting, absorbing and istropically scattering medium of thickness L (Figure 3). Initially, the medium is assumed to be cold at 0 K and initial intensities everywhere in the medium are zero. Then, at $t = 0$, the black bottom wall (z = 0) is subjected to a transient unit step function emissive power. The remaining walls are black and cold ($T = 0$). The optical thickness βL, and scattering albedo ω are 1 and 0.1, respectively. This problem is solved using the FTn FVM for both STEP and CLAM schemes. In this section, the dimensionless characteristic time step is defined as $\Delta t_c = 1/17$. The time evolutions of the radiative fluxes and radiation intensities as functions of time at three spatial locations and as functions of space at four times, respectively, are plotted to test the FTn FVM for both spatial STEP and CLAM schemes.
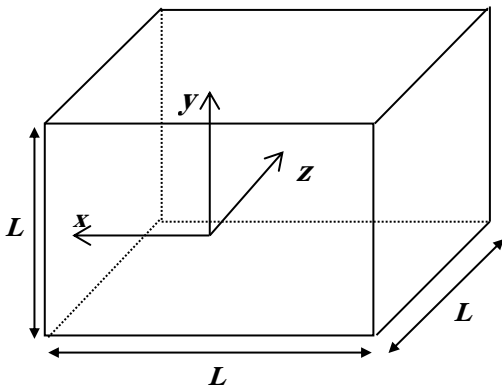

Figure 3 Schematic of a three-dimensional cube.

Effects of angular grids

To discuss the effects of angular grids on the results, the CLAM scheme, with 17×17×17 on spatial mesh, is used in all computations of this section. The reference solution was employed by Tan and Hsu using YIX method [13].

Figure 4 presents the effects of the angular grids on the incident radiation along the centerline of the medium at four instants $t/\Delta t_c$=4; 9; 15 and 49. It can be seen that the incident radiation, G, at a certain location of the medium increases with time. On the other hand, after $t/\Delta t_c$=49, the change of G versus time is invisible and the results reach to a steady state solutions. Assuming that the YIX method produces the most accurate solutions, the examination of figure 3 shows that the supply in precision of the angular scheme of the FTn FVM is remarkable. In fact, the FT10 FVM profiles coincide well with those of the reference solutions and the relative error lower than 2 %. Thus, using the FTn FVM with 180 control angles are sufficient to obtained accuracy results.

Figure 5 shows the radiative fluxes, q, distributions at four instants. It can be seen that the q distributions are similar to G distributions. Also, it can be shown that the fluxes along the center of the enclosure are more affected by both angular grids.

However, the fluxes near sides walls, for $z/L = 1/34$ and $z/L = 33/34$, do not change with these parameters.
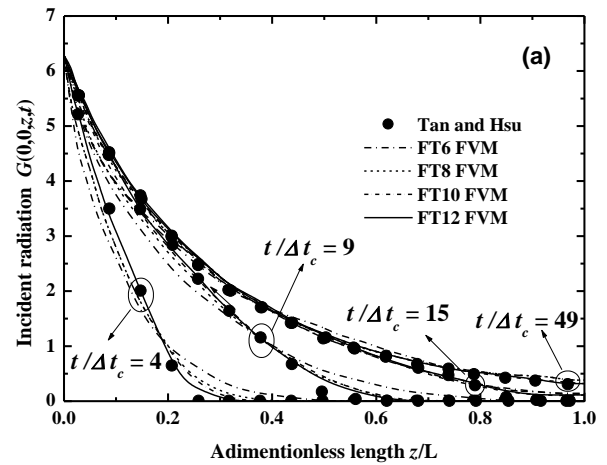

Figure 4 Effects of angular grids on the incident radiation distributions as function of time at different locations.
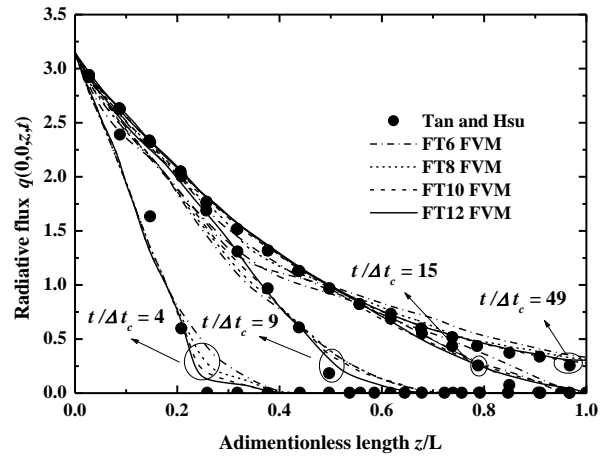

Figure 5 Effects of angular grids on the radiative flux along the centreline of the medium at different instants.

All calculations were performed using an Intel Pentium 4 processor at 3.06 GHz (512 RAM). The FT6 FVM requires less CPU-time than the FT8 FVM (743.3 s vs. 1114.4 s). Thus, it is found that when the total control angles increases, the CPU time is increased and it becomes strong using the FT12 FVM (2483.6 s).

Effects of spatial schemes

To discuss the effects of spatial schemes on the results, the FT8 FVM on angular mesh is used in all computations of this section.

Figure 6 shows that, when the CLAM scheme is used, the difference of incident radiation along the centerline of the medium between the fine mesh (17×17×17) and the coarse mesh (35×35×35) is very small. Thus, these results and the data of Tan and Hsu [13] are very close. However, the error is

larger and depends on location when using the same grids with the STEP scheme. Accordingly, the results from the step- using the fine grid and the results using the CLAM with coarse predictions are very close. Same conclusions can be made for the radiative heat flux predictions (figure does not plotted here).
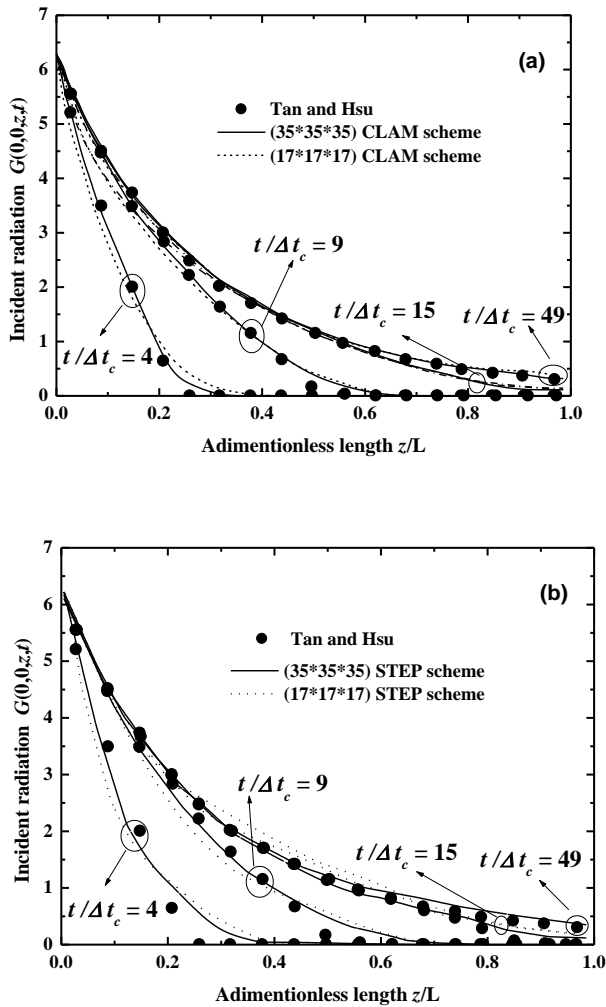

Figure 6 Effects of spatial schemes on the incident radiation distributions as function of time at three different locations.

It can be seen from Figure 6 that, at $t/\Delta t_c$=4 and $t/\Delta t_c$=9 (i.e. during the initial transient), false scattering is clearly noticed, especially where the STEP scheme is used. The STEP scheme over predicts the penetration depths and it is more significantly where STEP scheme is applied with a coarse spatial grid. These over-predictions decrease with spatial grid refinement and the error decreases from 11 to 4 %.

In conclusion, for all computations, the results for the coarse and fine grids are very close if the CLAM scheme is used. Furthermore, the predictions obtained using the STEP scheme show an influence of the grid size. For computational run time, it is noticed that, using the same grid, the STEP scheme is faster than the CLAM scheme. For a coarse grid, the CLAM and STEP schemes require 1114.4 and 932.5 s, respectively. However, Guedri and co-authors [6,7] demonstrate that the

difference of the CPU run times for STEP and CLAM schemes is reduced in the case of gray walls.

Effects of optical thickness

In this section, the FT10 FVM and the the coarse grid of the CLAM scheme are used. Figure 7 present the temporal evolution of the incident radiation for three optical thicknesses 0.1, 0.5 and 1 where unity value of the albedo scattering is consider. It can be seen that, at each instant in time, the heat flux distribution monotonically decreases with increasing optical thickness. With increasing optical thickness, the scattering effect is enhanced.
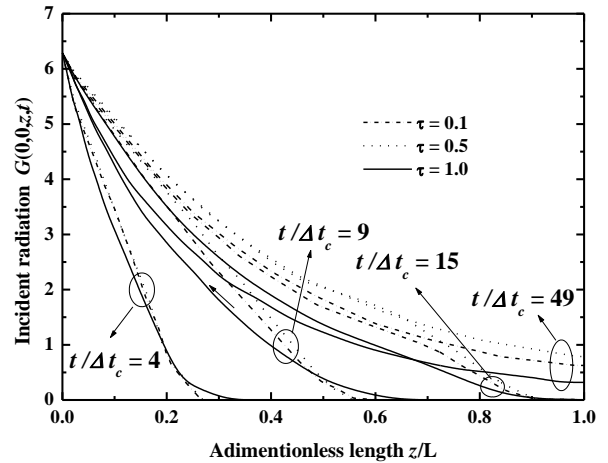

Figure 7 Incident radiation along the centreline in the z direction at different optical thickness.

Effects of scattering albedo

In the following, three values of the scattering albedo coefficient are considered to analyse their effects in the incident radiation along the centreline of the medium (Figure 8).
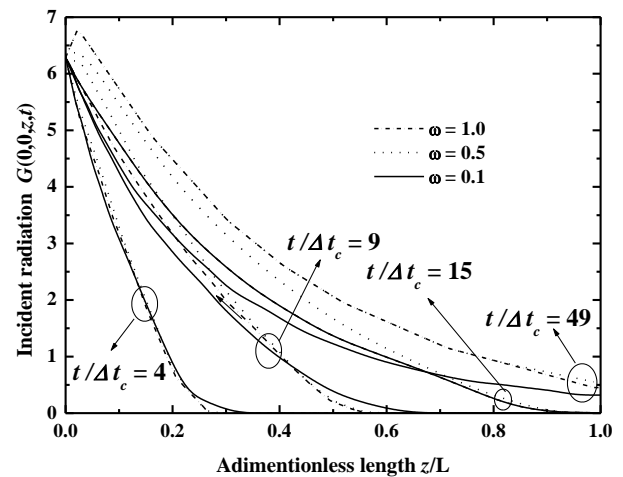

Figure 8 Incident radiation along the centreline in the z direction at different scattering albedos.

In these computations, the optical thickness is equal to 1 and the FT10 FVM and the coarse grid of the CLAM scheme are applied. At each instant in time, the incident radiation distribution increases with increasing scattering albedo. It is observed that the magnitude of incident radiation goes on increasing with the increased scattering albedo because there is more scattering in the medium.

CONCLUSION

In this work, the FTn finite volume method (FTn FVM) for transient radiative heat transfer is formulated, tested and investigated. The transient behavior of the three-dimensional absorbing, emitting and isotropically scattering medium is examined in terms of temporal and spatial evolutions of the radiative heat flux and incident radiation. Commonly used convection schemes in computational fluid dynamics (CFD) such as STEP and CLAM are introduced for spatial discetization of the transient radiative transfer equation (TRTE). The unsteady state solutions of the transient radiative model are validated against the data available in the literature. It is shown that the FTn FVM reduces largely the ray effects. Also, the false scattering is largely remedied using the CLAM scheme is applied for the angular discretization.

In all computations, the CLAM scheme produces more accurate results (with coarse grid) than the step scheme. Using the same (relatively coarse) spatial grid, the CLAM scheme captures the steep gradients and penetration depths more accurately than the step scheme.

Then, the effects of scattering albedo and the optical thickness on the incident radiation distributions are presented and discussed. As conclusion for this work, the FTn FVM using CLAM scheme is largely recommended to use in three-dimensional transient radiative heat transfer.

REFERENCES

[1] Modest M. F., Radiative Heat Transfer, McGraw-Hill, New York, 1993.

[2] Jaunich M., Raje S., Kim K., Mitra K., Guo Z., Bio-heat transfer analysis during short pulse laser irradiation of tissues, *International Journal of Heat and Mass Transfer*, Vol. 51, 2008, pp. 5511-5521.

[3] Jiao J., Guo Z., Modeling of ultra-short pulsed laser ablation in water and biological tissues in cylindrical coordinates, Appl. Phys B, vol 103, 2011, pp. 195-205.

[4] Sakami M., Mitra K., Hsu P.F., Analysis of light-pulse transport through two-dimensional scattering and absorbing media. *J. Quant. Spectrosc. Radiat. Transfer*, vol. 73, 2002, pp. 169–179.

[5] Kumar S., Mitra K, Microscale aspects of thermal radiation transport and laser application, *Adv Heat Transfer*, Vol 33, 1999, pp. 187–294.

[6] Guedri K., Borjini M. N., Me´chi R., and Said R., Formulation and Testing of the FTn Finite Volume Method for Radiation in 3-D Complex Inhomogeneous Participating Media, *J. Quant. Spectrosc. Radiat. Transfer*, vol. 98, 2006, pp. 425–445.

[7] Borjini M. N., Guedri K., Said R., Modeling of Radiative Heat Transfer in 3-D Complex Boiler with Non-Gray Sooting Media, *J. Quant. Spectrosc. Radiat. Transfer*, vol. 105, 2007, pp. 167–179.

[8] Kim S. H., Huh K. Y., A new angular discretization scheme of the finite volume method for 3-D radiative heat transfer in absorbing, emitting and anisotropically scattering media, *Int J Heat Mass Transfer*, vol. 43, 2000, pp. 1233–1242.

[9] Chai J.C., Transient radiative transfer in irregular two-dimensional geometries. *J Quant Spectrosc Radiative Transfer* vol 84, 2004, pp. 281–294.

[10] Chai J.C., Hsu P.F., Lam Y.C., Three-dimensional transient radiative transfer modelling using the finite-volume method, *J Quant Spectrosc Radiative Transfer*, vol. 86, 2004, pp. 299–313.

[11] Coelho P.J., Bounded skew high-order resolution schemes for the discrete ordinates method, *J Computational Physics*, vol. 175 (2), 2002, pp0 412 - 437.

[12] Coelho P.J., The role of ray effects and false scattering on the accuracy of the standard and modified discrete ordinates methods, *J Quant .Spectrosc Radiative Transfer*, vol.73, 2002, pp. 231–238.

[13] Tan Z. M., Hsu P.F., Transient radiative transfer in three-dimensional homogeneous and non-homogeneous participating media. *J. Quant. Spectrosc. Radiat. Transfer*, vol. 73, 2002, pp. 181–194.